Proceedings of the 2014 IEEE
International Conference on Robotics and Biomimetics
December 5-10, 2014, Bali, Indonesia

Dynamics of a Quadruped Robot during Locomotion

Xiaoqi Li, Wei Wang, Jianqiang Yi, and Hongjian Zhang

Abstract—**In this paper we analyze characteristics of the ground reaction force (GRF) experienced by the legs of the quadruped robot during stance phase in walk gait, in particular, when the height of center of gravity (COG) of the quadruped robot is changeable. We also build the dynamics model of the quadruped robot. Two dynamics equations during swing phase and stance phase are established, respectively. Additionally, we design a controller to adjust the height of COG of the quadruped robot. The controller uses the central pattern generator (CPG) model to generate basic rhythmic motion, and utilizes the discrete tracking differentiator (TD) to implement the transition between two different rhythmic medium values of the CPG. The combination of the CPG model and the discrete TD enables the quadruped robot to adjust the height of COG according to the environment. The ground reaction peak force and the joint torque of the quadruped robot increase with the reduction of the height of COG. Finally, we give a simulation example and the results, including an analysis of the vertical reaction force and the joint torque of the quadruped robot.**

I. Introduction

Quadruped robots are expected to be employed for a variety of dangerous and dirty tasks in fields like search and rescue in the future because of their superior mobility in rough and unstructured terrain. Therefore, significant effort has been made in enhancing the adaptivity of quadruped robots to nature environment. A modular controller which consists of a CPG model, stumbling correction reflex and virtual model is presented to utilize quadruped locomotion over unperceived rough terrain [1]. A reactive controller framework which comprises two main modules: one related to the generation of elliptic trajectories for the feet and the other for control of the stability of the whole robot, is designed to cope with terrain irregularities, trajectory tracking errors and poor state estimation [2]. A new approach for creating a continuously adjustable, smooth COG trajectory is proposed for quadruped robots to successfully traverse rough terrain [3].

In order to enable the quadruped robot to adapt to rough terrain, we are motivated to investigate the GRF experienced by the quadruped legs and joint torque of the quadruped robot during locomotion with changeable height of its COG. Lots of investigations have been done focusing on dynamics of legged robots. Michael Mistry et al. implement the inverse dynamics control of the floating-base systems which relates the world coordinate system to the global environment [4]. Bin Li et al. propose a novel dynamics model which supposes two different models according to the leg's state [5]. Wei Wang et al. investigate the mediolateral reaction forces during straight walking and turning [6].

While there is a lot of work addressing locomotion in rough terrain, research about some nature environment, for example, tight space, the ice surface, is relatively rare. In these situations, a quadruped robot should lower the height of its COG to guarantee maneuverability and stability.

The main thrust of this paper is to build the dynamics model of a quadruped robot and analyze the dynamics characteristics of the GRF and joint torque for investigating walking with different height of COG using a simulated model, but with biologically-based assumptions.

To achieve this goal, the first objective of this work is to develop a controller that can be used to adjust the height of COG. The controller utilizes the CPG model to generate the rhythmic motion and the discrete TD to implement the transition between two different rhythmic medium values of the CPG, so as to adjust the height of COG of the quadruped robot.

CPG observed in animals has been a major source of inspiration for trajectory generation in quadruped robots. Tekken2 [7] can walk with medium forward speed on irregular terrains in outdoor environments using a neural system model consisting of a CPG, responses and reflexes. Simulated robots iCub, Aibo and Ghostdog [8] show that adding sensory feedback in the CPG allows for more robust locomotion.

In this contribution, we reveal the characteristics of the GRF and create the dynamics model of a quadruped robot. A controller, based on the CPG model and the discrete TD, is designed to realize the rhythmic motion and the adjustment of the height of COG. In addition, we analyze and compare the simulation results including the GRF and joint torque of a quadruped robot.

In the remainder of the paper, we firstly analyze the GRF and build the dynamics model. Following this, the controller which combines the CPG model and the discrete TD is presented. Then, the quadruped model and setup are introduced. Finally, simulation results are analyzed and contrasted.

II. The Ground Reaction Force And Dynamics Model

A. Ground Reaction Force

Like the biological locomotion [9], when the toe of a

Manuscript received July 21, 2014. This work was supported in part by the National Natural Science Foundation of China under Grant 61375101 and 61421004. The authors Xiaoqi Li, Wei Wang and Jianqiang Yi are with the Institute of Automation, Chinese Academy of Sciences, 95 Zhongguancun East Road, Beijing, 100190, China (e-mail: {xiaoqi.li, wei.wang, jianqiang.yi}@ia.ac.cn). The author Hongjian Zhang is with Beijing Aerospace Automatic Control Institute, Beijing, 100854, China (e-mail: colin_167@163.com).

978-1-4799-7397-2/14/$31.00 © 2014 IEEE

quadruped robot contacts with the ground, the quadruped robot applies forces to the ground through that toe for supporting and moving its body on the ground. The toe then experiences the GRF which is equal in magnitude and opposite in direction to the force exerted by the toe. The GRF, a necessary force for the quadruped robot for locomotion, is the vector sum of the vertical (V) force, fore-aft (FA) force, and mediolateral (ML) force, and produces bending moments along the leg, as shown in Fig. 1. The three components of the GRF have the following characteristics [10]:

1) The V force and FA force are main components compared to ML force in magnitude and V peak force occasionally exceeds FA peak force.
2) The FA force is a braking force when it is opposite in direction to the movement, on the contrary a propulsive force.
3) Compared to the V and FA components, the ML component of the GRF is trivial in magnitude yet it contributes requisite for the turning maneuver [6].

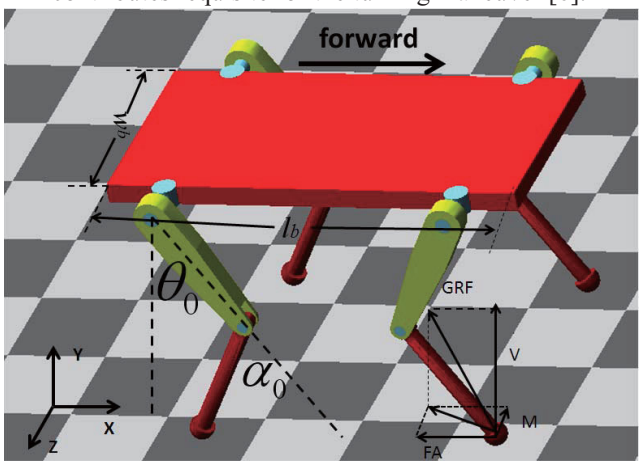

Fig. 1. GRF of the right-fore toe in a quadruped robot. V, ML, and FA forces, three components of the GRF, represent the vertical reaction force, the mediolateral force and the fore-aft force, respectively.

B. The Inverse Dynamics

The inverse dynamics is the calculation of the forces or torques required at a robot's joints to deliver a required motion trajectory which encompasses a set of joint positions, velocities and accelerations. In trajectory planning, we can use the inverse dynamics to check and ensure that a designed trajectory can be achieved within the actuators' limits.

The quadruped robot is a floating-base system whose base is not fixed to the environment but free to move. In recent literature [11], the inverse dynamics control adds a fixed base to the system which is attached to the quadruped robot via 6 virtual DOFs. The computational complexity of this approach is high because of extra computation on the virtual DOFs and consequently, we consider building a dynamics model without need to calculate the extra virtual DOFs.

Each leg of the quadruped robot is regarded as a separated and serial manipulator, consisting of a virtual body and a leg of the quadruped robot [5], as shown in Fig. 2. A stride cycle is defined as two stages: the swing phase and the stance phase.

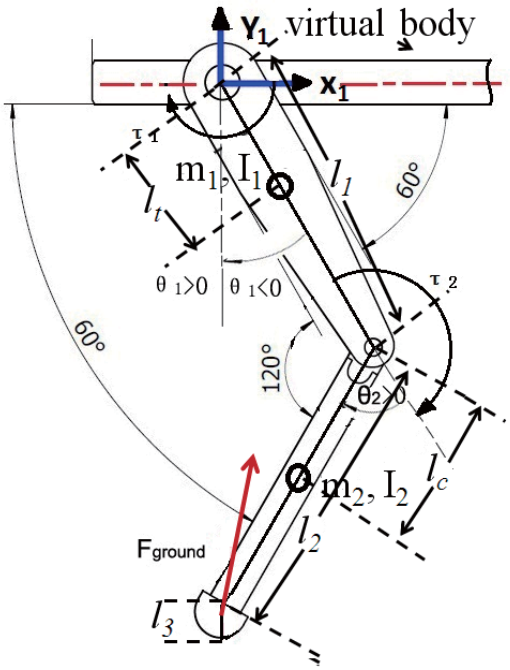

Fig. 2. One leg is regarded as a serial manipulator with definition of variables for the inverse dynamics model.

We build the inverse dynamics model apart in stance phase and swing phase because of their different constraint conditions. This modeling approach is convenient because there is no need to calculate the extra virtual joints. We will demonstrate the inverse dynamics model of one leg.

B.1) Dynamics Equations for Swing Phase

When the leg is in swing phase which means the toe has no contact with the ground, we assume the virtual body is not move and suppose it as the base. The base frame is established at the hip joint, as shown in Fig. 2.

To derive the dynamics equations of motion of a serial manipulator in swing phase following the Lagrangian approach [12], we first write the Lagrangian

$$L = E_K - E_P \tag{1}$$

where E_K is the kinetic energy and E_P is the potential energy of the serial manipulator. Velocities of the thigh and shank can be obtained by the following equations

$$r_t = \begin{bmatrix} x_t \\ y_t \end{bmatrix} = \begin{bmatrix} -l_t \sin\theta_1 \\ -l_t \cos\theta_1 \end{bmatrix} \tag{2}$$

$$r_c = \begin{bmatrix} x_c \\ y_c \end{bmatrix} = \begin{bmatrix} -l_1 \sin\theta_1 - l_c \sin h \\ -l_1 \cos\theta_1 - l_c \cos h \end{bmatrix} \tag{3}$$

$$v_t^2 = \dot{x}_t^2 + \dot{y}_t^2 = \dot{\theta}_1 l_t^2 \tag{4}$$

$$v_c^2 = \dot{x}_c^2 + \dot{y}_c^2 = \dot{\theta}_1^2 l_1^2 + (\dot{\theta}_1 + \dot{\theta}_2)^2 l_c^2 + 2\dot{\theta}_1 l_1 l_c \cos(\theta_1 - h) \tag{5}$$

where the definition of θ_1 and θ_2 are shown in Fig. 2. $h = \theta_1 + \theta_2$. l_1 is the length of the thigh. l_t and l_c are the distance from the hip joint to the COG of the thigh and the distance from the knee joint to the COG of the shank,

respectively. r_t, r_c are positions of the COG of the thigh and shank, respectively. v_t, v_c are velocities of the COG of the thigh and shank, respectively.

The kinetic energy of the serial manipulator is computed by using the equation

$$\begin{aligned} E_K &= E_{kt} + E_{kc} = \frac{1}{2} m_1 {v_t}^2 + \frac{1}{2} m_2 {v_c}^2 \\ &= \frac{1}{2}\dot{\theta}_1^2 (m_1 l_t^2 + m_2 l_1^2 + I_{1zz}) + \frac{1}{2}(\dot{\theta}_1 + \dot{\theta}_2)^2 (m_2 l_c^2 \\ &\quad + I_{2zz}) + \dot{\theta}_1 (\dot{\theta}_1 + \dot{\theta}_2) m_2 l_1 l_c \cos\theta_2 \end{aligned} \tag{6}$$

Here E_K, E_{kt} and E_{kc} are the kinetic energy of the serial manipulator, the thigh and the shank, respectively. m_1 and m_2 are the mass of the thigh and the shank, respectively. The position of COG of thigh and shank are shown in Fig. 2. I_{1zz} and I_{2zz} represent principal moment of inertia perpendicular to the z-axial direction of the thigh and shank link, respectively.

The potential energy of the serial manipulator is equal to the work required to transport the COG of each link from a reference plane to a given position. This can be written as

$$E_{pt} = -g m_1 l_t \cos\theta_1 \tag{7}$$

$$E_{pc} = -g m_2 (l_1 \cos\theta_1 + l_c \cos h) \tag{8}$$

$$E_p = E_{pt} + E_{pc} = -g m_1 l_t \cos\theta_1 - g m_2 (l_1 \cos\theta_1 + l_c \cos h) \tag{9}$$

where E_p, E_{pt} and E_{pc} are the potential energy of the serial manipulator, the thigh and the shank, respectively. g is the gravitational acceleration.

Thus, using these expressions for the kinetic and potential energies, we can substitute the Lagrangian L into the Euler-Lagrange equation

$$\tau_i = \frac{d}{dt}\frac{\partial L}{\partial \dot{\theta}_i} - \frac{\partial L}{\partial \theta_i} \qquad i = 1,2 \tag{10}$$

which is expanded by symbolic differentiation to give the generalized torques τ_i, for i=1,2, in terms of the generalized joint positions, velocities and accelerations.

The equation can be put into a closed form compact vector-matrix notation as

$$\begin{bmatrix} \tau_1(t) \\ \tau_2(t) \end{bmatrix} = B(\theta) \begin{bmatrix} \ddot{\theta}_1(t) \\ \ddot{\theta}_2(t) \end{bmatrix} + C(\theta, \dot{\theta}) \begin{bmatrix} \dot{\theta}_1(t) \\ \dot{\theta}_2(t) \end{bmatrix} + D(\theta) \tag{11}$$

where

$$B(\theta) = \begin{pmatrix} b_1 & b_2 \end{pmatrix}$$

$$b_1 = \begin{pmatrix} m_1 l_t^2 + m_2 (l_1^2 + l_c^2 + 2 l_1 l_c \cos\theta_2) + I_{1zz} + I_{2zz} \\ m_2 (l_c^2 + l_1 l_c \cos\theta_2) + I_{2zz} \end{pmatrix}$$

$$b_2 = \begin{pmatrix} m_2 (l_c^2 + l_1 l_c \cos\theta_2) + I_{2zz} \\ m_2 l_c^2 + I_{2zz} \end{pmatrix}$$

$$C(\theta, \dot{\theta}) = \begin{pmatrix} -\dot{\theta}_2 m_2 l_1 l_c \sin\theta_2 & -(\dot{\theta}_1 + \dot{\theta}_2) m_2 l_1 l_c \sin\theta_2 \\ \dot{\theta}_1 m_2 l_1 l_c \sin\theta_2 & 0 \end{pmatrix}$$

$$D(\theta) = \begin{pmatrix} g m_1 l_t \sin\theta_1 + g m_2 l_1 \sin\theta_1 + g m_2 l_c \sin h \\ g m_2 l_c \sin h \end{pmatrix}$$

Here $\tau_1(t)$ and $\tau_2(t)$ are torques of the hip joint and the knee joint, respectively. The $B(\theta)$ is the generalized inertia matrix of the serial manipulator, $C(\theta, \dot{\theta})$ is a matrix which contains the Coriolis and centrifugal forces, and $D(\theta)$ is the gravity force vector.

B.2) Dynamics Equations for Stance Phase

When the leg is in stance phase, the leg pushes down the ground and receives reactive force, which we call GRF, as shown in Fig. 2. We utilize GRF to build the inverse dynamics model in stance phase. The origin of the reference frame is located at the hip joint, as shown in Fig. 2. The position of the toe in the reference frame is represented as follows:

$$r_f = \begin{bmatrix} x_f \\ y_f \end{bmatrix} = \begin{bmatrix} -l_1 \sin\theta_1 - l_2 \sin(\theta_1 + \theta_2) \\ -l_1 \cos\theta_1 - l_2 \cos(\theta_1 + \theta_2) - l_3 \end{bmatrix} \tag{12}$$

where r_f represents the position of the toe. l_2 is the length of the shank. l_3, shown in Fig. 2, is approximately the radius of the toe.

We use the chain rule to calculate partial derivates, then divide both sides by the differential time element, and get:

$$\dot{r}_f = J \cdot \dot{\theta}_i \qquad i = 1,2 \tag{13}$$

$$J = \begin{pmatrix} -l_1 \cos\theta_1 - l_2 \cos(\theta_1 + \theta_2) & -l_2 \cos(\theta_1 + \theta_2) \\ l_1 \sin\theta_1 + l_2 \sin(\theta_1 + \theta_2) & l_2 \sin(\theta_1 + \theta_2) \end{pmatrix}$$

where J is the Jacobian. According to Jacobian in the force domain [12], the inverse dynamics model of the serial manipulator in stance phase is given by

$$\begin{bmatrix} \tau_1(t) \\ \tau_2(t) \end{bmatrix} = J^T \cdot F_{Ground} = \begin{pmatrix} E(\theta_1, \theta_2) \\ F(\theta_1, \theta_2) \end{pmatrix} \tag{14}$$

where

$$\begin{aligned} E(\theta_1, \theta_2) &= -l_1 \cos\theta_1 - l_2 \cos(\theta_1 + \theta_2) F_x \\ &\quad + l_1 \sin\theta_1 + l_2 \sin(\theta_1 + \theta_2) F_y \end{aligned}$$

$$F(\theta_1, \theta_2) = -l_2 \cos(\theta_1 + \theta_2) F_x + l_2 \sin(\theta_1 + \theta_2) F_y$$

Here F_{Ground} is the GRF, as shown in Fig. 2. F_x and F_y are components of the GRF in the x-axial direction and the y-axial direction, respectively.

III. Hopf Oscillator And The Discrete Tracking-differentiator

To enable the quadruped robot to traverse through tight space and keep stability, we propose a controller to adjust the height of COG of the quadruped robot. The controller combines the rhythmic locomotion and the rhythmic medium value adjustment by adding adjustment trajectory to rhythmic signals. The rhythmic locomotion and adjustment trajectory are generated by the CPG model and the discrete TD, respectively.

A. The CPG Model

The CPG is employed to generate the fundamental rhythmic motion in locomotion without sensory feedback and without any inputs. The Hopf oscillator, as a model of CPG, is adopted to generate control signals for locomotion. The Hopf oscillator is a kind of nonlinear oscillator with high stability and strong phase locking feature so as to be stable against perturbation. The amplitude and frequency can be modulated by simple parameter change. The Hopf oscillator is represented by the following equations [8]:

$$\dot{n} = \alpha(\mu - r^2)n - \omega o \tag{15}$$

$$\dot{o} = \alpha(\mu - r^2)o + \omega n \tag{16}$$

$$\omega = \frac{\omega_{\text{swing}}}{e^{bo}+1} + \frac{\omega_{\text{stance}}}{e^{-bo}+1} \tag{17}$$

where $r = \sqrt{n^2 + o^2}$ and n and o are state variables. $\sqrt{\mu}$ is the amplitude of the oscillations (for $\mu > 0$). $w\,(rad \cdot s^{-1})$, determined by ω_{swing} and ω_{stance} which control the frequency of swing and stance phase, is the frequency of the oscillation. We can independently control the frequencies of the ascending and descending phases of the oscillation by modifying ω_{swing} and ω_{stance}, respectively. α is a positive constant that controls the speed of convergence which becomes large with the increase of α.

We utilize four Hopf oscillators to generate control signals for hip joints. The four Hopf oscillators are mutually entrained by connecting the CPG of each leg with coupling coefficients to generate desired gait. The coupled CPG oscillates in the same period with a fixed phase difference, which results in a gait, such as walk gait, trot gait, etc. We use the coupled Hopf oscillators to generate the walk gait, shown as the following [8]:

$$\dot{n}_i = \alpha(\mu_i - r_i^2)n_i - \omega o_i \tag{18}$$

$$\dot{o}_i = \alpha(\mu_i - r_i^2)o_i + \omega n_i + \sum k_{ij} o_j \tag{19}$$

Here i and j denote the ith and jth oscillators, respectively. k_{ij}, the coupling coefficient, which determines the type of gait, is specified by the coupling matrices. The other parameters are defined as before.

B. The Discrete Tracking-differentiator

To change the height of COG of the quadruped robot, we are required to realize smooth transition between two different rhythmic medium values for walking stability. The discrete TD is then typically used to track dynamic characteristics of the input as soon as possible, and in the meantime, generate approximate differential signal. We devote to utilize the discrete TD to realize smooth transition between two different rhythmic medium values. The discrete TD is shown as follows [13], [14]:

$$v_1(k+1) = v_1(k) + hv_2(k) \tag{20}$$

$$v_2(k+1) = v_2(k) + hfh \tag{21}$$

$$fh = fhan(v_1 - v, v_2, r, h) \tag{22}$$

where v_1 is the desired trajectory and v_2 is its derivative. v and h are the input and the step size, respectively. r determines the speed of the transition which becomes faster as the parameter r increases, and $fhan(v_1, v_2, r, h)$ is defined as [13], [14] .

Fig. 3 (blue, dashed line) depicts the adjustment trajectory which realizes smooth transition between two different rhythmic medium values. The red line shows the input discrete rhythmic medium values v. the output v_1 can track the set value v arbitrarily fast as long as r is chosen arbitrarily large without any overshoot.

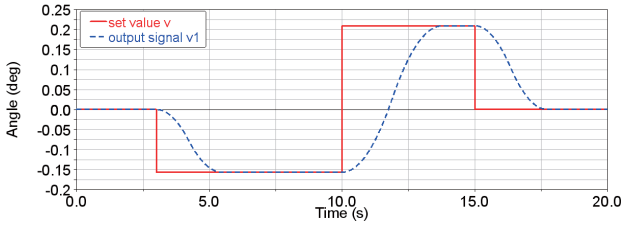

Fig. 3. The red line shows the input discrete rhythmic medium values, and the blue dashed line depicts that the output signal v_1 tracks the set value v smoothly.

IV. The Quadruped Model And Simulation Setup

The quadruped model used in our simulation consists of a body and four legs, as shown in Fig. 1. Each leg connects to the body by the hip pitch joint, and includes the thigh link and the shank link which are connected together by the knee pitch joint. The quadruped model is 1.05m in length and 0.69m in width. The total weight of the robot is 50.0Kg. The initial value of hip joint θ_0 and knee joint α_0 are 30 degrees and 60 degrees, respectively. The corresponding parameters, labeled in Fig. 1 and Fig. 2, are listed in Table I.

TABLE I
PARAMETERS FOR THE QUADRUPED MODEL

Symbol	Quantity	Symbol	Quantity
l_b	1.05m	w_b	0.69m
l_1	0.35m	l_2	0.35m
l_3	0.09m	l_t	0.175m
l_c	0.175m	m_1	3.5kg
m_2	2.0kg	I_{1zz}	2738.792kg·mm^2
I_{2zz}	401.731 kg·mm^2		

The simulation is performed in MSC.ADAMS simulation platform. The rationality of parameters setting plays an important role in the control of the quadruped model. To compute the impact force and the friction force between toes of the quadruped robot and the ground, we set impact force parameters and friction parameters, shown in Table II.

TABLE II
IMPACT FORCE PARAMETERS AND FRICTION PARAMETERS

impact force parameters		friction parameters	
Symbol	Quantity	Symbol	Quantity
Stiffness (N/m)	1.0E+008	Mu Static	1.0
Damping (Ns/m)	1.0E+004	Mu Dynamic	0.5
Exponent	2.2	Stiction Transition Velocity (m/s)	0.1
		Friction Transition Velocity (m/s)	1.0

The controller is implemented in *MATLAB/Simulink*, and controls the quadruped model in MSC.ADAMS by using the dynamic-link library in *MATLAB/Simulink*. The sample time is 1e-3 s. We simulate two scenarios: the quadruped robot walks with a COG height of 0.606 m and with a COG height of 0.577 m. The control signals for hip joints and knee joints in two scenarios described in section III are shown in Fig. 4 and Fig. 5. The abbreviations LF, LH, RF and RH represent left fore, left hind, right fore, and right hind, respectively.

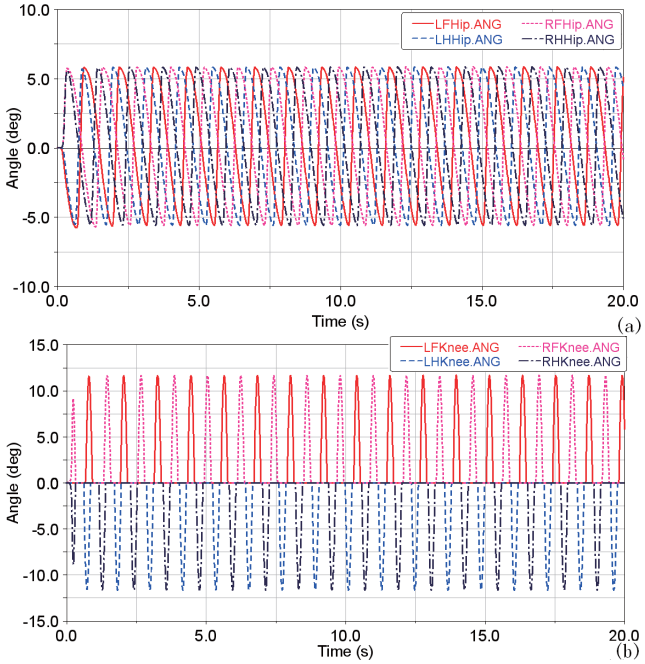

Fig. 4. (a) The control signals of hip joints of the quadruped model with a COG height of 0.606 m. (b) The control signals of knee joints of the quadruped model with a COG height of 0.606 m.

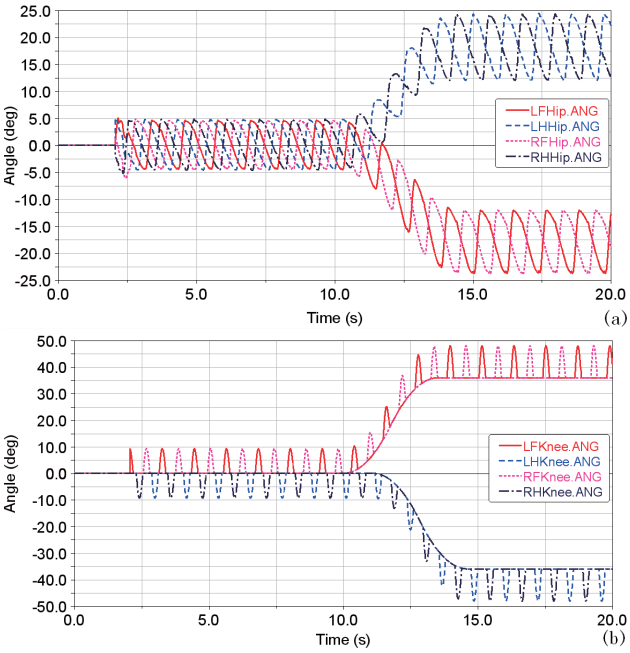

Fig. 5. (a) The control signals of hip joints of the quadruped model with a COG height of 0.577 m. (b) The control signals of knee joints of the quadruped model with a COG height of 0.577 m.

V. Simulation Results And Discussion

In order to contrast the V forces and joint torques of the quadruped robot walking with different height of COG, we show the simulation results in the period of 15 s to 20 s.

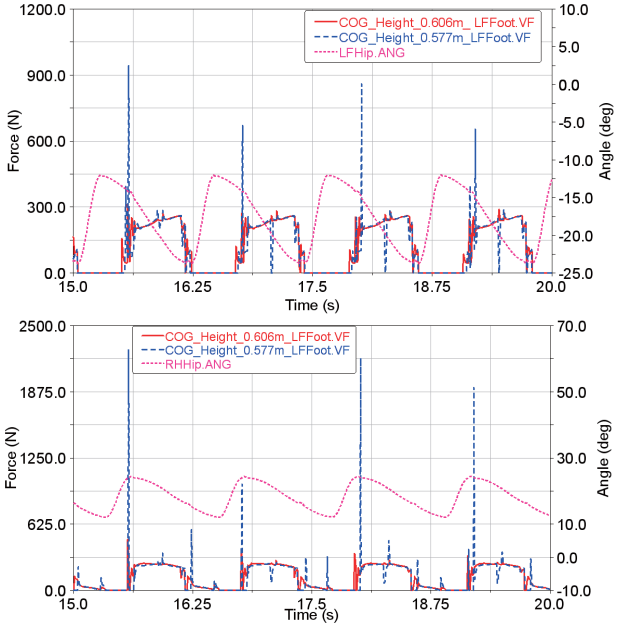

Fig. 6. V forces of LF and RH legs of the quadruped model with a COG height of 0.606 m and with a COG height of 0.577 m, respectively.

The V forces, shown in Fig. 6, take large responsibility for generating the pitch moments during stance phase. Some observations on characteristics of the V forces of the quadruped model with a COG height of 0.606 m and with a COG height of 0.577 m from our study are discussed as follows:

1) During walking with a COG height of 0.606 m and with a COG height of 0.577 m, the two legs experience V forces during stance phase. There are V force pulses at the beginning of stance phase because the toe crashes with the ground.
2) During walking with a COG height of 0.606 m, the V peak forces are within 600.0 N, or about 1.2 times the total weight, as listed in Table I. This force level agrees with the measurements of trotting HyQ, up to 1.2 times body weight exerted on each limb [15]. During walking with a COG height of 0.577 m, however, the LF and RH legs experience significantly larger V forces pulses up to 1200.0 N and 2500.0 N, respectively, and the V force of the RH leg is much larger than that of the LF leg.

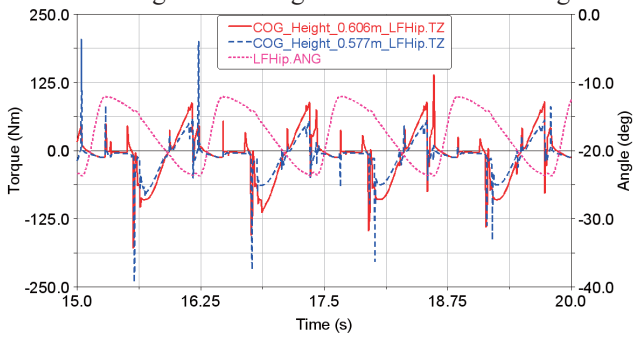

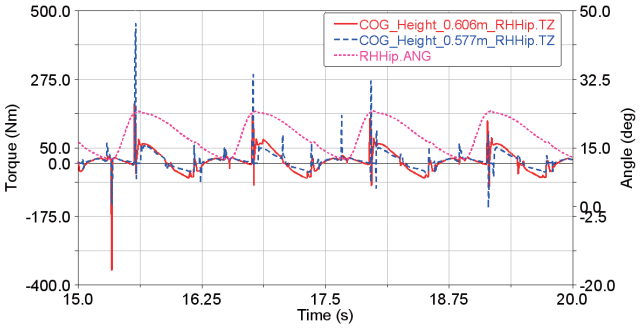

Fig. 7. Torques for the hip axes of LF and RH legs of the quadruped model with a COG height of 0.606 m and with a COG height of 0.577 m, respectively.

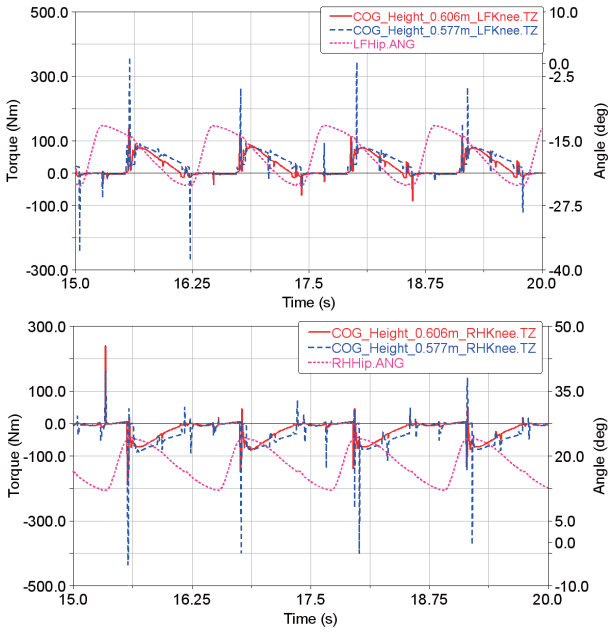

Fig. 8. Torques for the knee axes of LF and RH legs of the quadruped model with a COG height of 0.606 m and with a COG height of 0.577 m, respectively.

As shown in Fig. 7, during walking with a COG height of 0.606 m, the amplitude of the hip torque is in the range of -250 Nm to 250 Nm. However, during walking with a COG height of 0.577 m, the amplitude of the hip torque is much larger in the range of -400 Nm to 500 Nm.

The knee torques of the LF and RH legs of the quadruped model walking with a COG height of 0.606 m and a COG height of 0.577 m are shown in Fig. 8. Minimal torque is required to transfer the shank during swing phase because only the relatively small inertial load of the shank is seen. During stance, however, much larger torque is required, and V force is dominant as it has larger moment arm. During walking with a COG height of 0.606 m, the knee torque of the quadruped model is smaller than that during walking with a COG height of 0.577 m.

VI. Conclusion

This paper firstly analyzes the GRF and builds the inverse dynamics model of the quadruped robot in swing phase and stance phase respectively to simplify the computation. The inverse dynamics model facilitates to predict the torque needed to track the designed joint trajectory. Then we present the discrete TD which cooperates with the CPG model to fulfill the change of the height of COG in walk gait so that the quadruped robot can lower the height of COG to enhance stability and traverse through tight space. Finally, we carry out the controller on a simulated quadruped robot and analyze the simulation results. The analysis about GRF and joint torque are helpful to facilitate the mechanical design of quadruped robots.

Future work will be aimed at utilizing the inverse dynamics model to control the quadruped robot, and improving the controller considering the experimental results, and evaluating the controller on a real quadruped robot.

References

[1] Mostafa Ajallooeian, Soha Pouya, Alexander Sproewitz, and Auke J. Ijspeert, "Central Pattern Generators Augmented with Virtual Model Control for Quadruped Rough Terrain Locomotion," in *IEEE International Conference on Robotics and Automation*, Karlsruhe, Germany, pp. 3321-3328, 2013.

[2] Victor Barasuol et al., "A Reactive Controller Framework for Quadrupedal Locomotion on Challenging Terrain," in *IEEE International Conference on Robotics and Automation*, Karlsruhe, Germany, pp. 2554-2561, 2013.

[3] Dimitris Pongas, Michael Mistry, and Stefan Schaal, "A Robust Quadruped Walking Gait for Traversing Rough Terrain," in *IEEE International Conference on Robotics and Automation*, Roma, Italy, pp. 1474-1479, 2007.

[4] Michael Mistry, Jonas Buchli, and Stefan Schaal, "Inverse Dynamics Control of Floating Base Systems Using Orthogonal Decomposition," in *IEEE International Conference on Robotics and Automation*, Anchorage, USA, pp. 3406-3412, 2010.

[5] Bin Li, Yajuan Guo, Xuesong Shao, Wei Wang, and Jianqiang Yi, "Novel Inverse Dynamics Control Strategy with Different Phases for the Quadruped Robot," in *10th World Congress on Intelligent Control and Automation*, Beijing, China, pp. 3601-3606, 2012.

[6] Wei Wang and Yiping Yang, "Turning Maneuvers and Mediolateral Reaction Forces in a Quadruped Robot," in *IEEE International Conference on Robotics and Biomimetics*, Phuket, Thailand, pp. 515-520, 2011.

[7] Hiroshi Kimura, Yasuhiro Fukuoka, and Avis H. Cohen, "Adaptive Dynamic Walking of a Quadruped Robot on Natural Ground Based on Biological Concepts," *The International Journal of Robotics Research*, vol. 26, no. 5, pp. 475-490, 2007.

[8] Ludovic Righetti and Auke Jan Ijspeert, "Pattern Generators with Sensory Feedback for the Control of Quadruped Locomotion," in *IEEE International Conference on Robotics and Automation*, Pasadena, USA, pp. 819-824, 2008.

[9] B. Demes, K.J. Carlson, and T.M. Franz, "Cutting Corners: the Dynamics of Turning Behaviors in Two Primate Species," *The Journal of Experimental Biology*, vol. 209, pp. 927-937, 2006.

[10] K.J. Carlson, B. Demes, and T.M. Franz, "Mediolateral Forces Associated with Quadrupedal Gaits of Lemurids," *Journal of Zoology*, vol. 266, no. 3, pp. 261-273, 2006.

[11] Roy Featherstone, "Rigid Body Dynamics Algorithms," *Springer Science+ Business Media*, LLC., 2007.

[12] John J. Craig, *Introduction to Robotics: Mechanics and Control*. Addison-Wesley Publishing Co., pp. 145-149, 1989.

[13] Jingqing Han, "From PID to Active Disturbance Rejection Control," *IEEE Transactions On Industrial Electronics*, vol. 56, no. 3, pp. 900-906, 2009.

[14] Zhiqiang Gao, Yi Huang, and Jingqing Han, "An Alternative Paradigm For Control System Design," in *40th IEEE Conference on Decision and Control*, Orlando, USA, pp. 4578-4585, 2001.

[15] Claudio Semini et al., "HyQ-A Dynamic Locomotion Research Platform", Available: http://www.iit.it/en/advanced-robotics/hyq.html.